

Accepted refereed manuscript of:

Markovsky C, Byrne JM, Lalla E, Lozano-Gorrin AD, Klingelhoefer G, Rull F, Kappler A, Hoffmann T & Schröder C (2017) Abiotic versus biotic iron mineral transformation studied by a miniaturized backscattering Mössbauer spectrometer (MIMOS II), X-ray diffraction and Raman spectroscopy, *Icarus*, 296, pp. 49-58.

DOI: [10.1016/j.icarus.2017.05.017](https://doi.org/10.1016/j.icarus.2017.05.017)

© 2017, Elsevier. Licensed under the Creative Commons Attribution-NonCommercial-NoDerivatives 4.0 International
<http://creativecommons.org/licenses/by-nc-nd/4.0/>

Manuscript Details

Manuscript number	ICARUS_2016_477
Title	Abiotic versus biotic iron mineral transformation studied by a miniaturized backscattering Mössbauer spectrometer (MIMOS II), X-ray diffraction and Raman spectroscopy
Article type	Research paper

Abstract

Searching for biomarkers or signatures of microbial transformations of minerals is a critical aspect for determining how life evolved on Earth, and whether or not life may have existed in other planets, including Mars. In order to solve such questions, several missions to Mars have sought to determine the geochemistry and mineralogy on the Martian surface. This research includes the two miniaturized Mössbauer spectrometers (MIMOS II) on board the Mars Exploration Rovers Spirit and Opportunity, which have detected a variety of iron minerals on Mars, including magnetite ($\text{Fe}_2+\text{Fe}_3+2\text{O}_4$) and goethite ($\alpha\text{-FeO(OH)}$). On Earth, both minerals can derive from microbiological activity (e.g. through dissimilatory iron reduction of ferrihydrite by Fe(III)-reducing bacteria). Here we used a lab based MIMOS II to characterize the mineral products of biogenic transformations of ferrihydrite to magnetite by the Fe(III)-reducing bacteria *Geobacter sulfurreducens*. In combination with Raman spectroscopy and X-ray diffraction (XRD), we observed the formation of magnetite, goethite and siderite. We compared the material produced by biogenic transformations to abiotic samples in order to distinguish abiotic and biotic iron minerals by techniques that are or will be available onboard Martian based laboratories. The results showed the possibility to distinguish the abiotic and biotic origin of the minerals. Mossbauer was able to distinguish the biotic/abiotic magnetite with the interpretation of the geological context (Fe content mineral assemblages and accompanying minerals) and the estimation of the particle size in a non-destructive way. The Raman was able to confirm the biotic/abiotic principal peaks of the magnetite, as well as the organic principal vibration bands attributed to the bacteria. Finally, the XRD confirmed the particle size and mineralogy

Keywords Bio-magnetite; Mössbauer spectroscopy; Raman spectroscopy; iron oxides; XRD

Corresponding Author Emmanuel Lalla

Corresponding Author's Institution Extreme Light Infrastructure (ELI) – Nuclear Physics, IFIN–HH

Order of Authors Cristina Markovski, James M. Byrne, Emmanuel Lalla, A. Diego Lozano-Gorrin, Goestar Klingelhofer, Fernando Rull, Andreas Kappler, Thorsten Hoffmann, Christian Schröder

Suggested reviewers Fernando Gazquez, Pablon Sobron, Jung-Fu Lin, Jose J. Velazquez Garcia, Alejandro Rodriguez-Navarro

Submission Files Included in this PDF

File Name [File Type]

Letter to the Editor_Final.docx [Response to Reviewers]

Highlight.docx [Highlights]

Manuscript_Final.docx [Manuscript File]

List of Figures_Final.docx [Figure]

Figure-1.tif [Figure]

Figure-2.tif [Figure]

Figure-4.tif [Figure]

List of Tables_Final.docx [Table]

Submission Files Not Included in this PDF

File Name [File Type]

Figure-3.PNG [Figure]

To view all the submission files, including those not included in the PDF, click on the manuscript title on your EVISE Homepage, then click 'Download zip file'.

Dear Ms Scalzo,

We thank you for your efforts in helping during the review process of this manuscript. We have carefully considered all the points which have been raised by the reviewer and feel that they have contributed to improving the quality of the manuscript. The details of our changes are included herewith:

Reviewer (Minor corrections)

→ *We appreciate the time and effort the reviewer has taken to evaluate the manuscript and are pleased with their opinion.*

We have considered the modifications that you recommended along the paper such as experimental campaigning to experiments, minor corrections on the references, small vocabulary corrections, etc.

Line 38: With the interpretation of the geological context and

We have added the geological context: (Fe content mineral assemblages and accompanying minerals).

Line 158: in situ measurements were carried out which correspond to samples where Mössbauer data was collected throughout the course of the experiment.

We rephrased the sentence in simple way: *in situ* Mössbauer measurements were carried out throughout the course of the experiment on each samples and its preparation.

Line 209: You could say here in which region of the spectrum

Based on the nature of Mössbauer spectroscopy, it is not common to refer to specific regions within a spectrum (e.g. as is the case for Raman), but instead discuss the presence of doublets or sextets. Therefore, we do not think defining the specific region of the spectrum will improve the interpretation of the data.

Line 212: You could say here in which region of the spectrum

See comment above

Line 296: Can you competently rule out the presence of remainders from the growth medium?

We removed this part by mentioning the existence of the organic substances due to the biochemical process.

Line 311: MIMOS II instrument, with the in situ experiments only looking at the very bottom layer of the iron layer which was undergoing microbial transformation. Is it possible that some conversion happens during the filtering stage?

The filtering removed the liquid fraction of the media which contains dissolved salts and the electron donor within a time frame of under 5 minutes. Consequently, there are no microbial transformation processes which could take place during or after filtration of the samples. As samples were measured directly after filtration under anoxic conditions, we do not consider that further crystallization took place in the samples.

Line 359: FH-AQDS-13 is calculated to be higher than those previously reported. Is there an implication for this?

We clarified by adding on the sentence: “..and showing a higher concentration of ferrous magnetite.”

Figure 3. It has been corrected and improved.

Table 1. What is the difference between these two rows of "magnetite nanophases"? You may explain it in the table caption.

We have updated the figure caption to include:

^aSuperparamagnetic magnetite - magnetic ordering prevented by small particle size.

^bMagnetically ordered magnetite that has not reached full hyperfine splitting because of small particle size and/or impurities

^cValues from Morris et al. (2008), averaging all magnetite and goethite measurements obtained in Gusev Crater with Mars Exploration Rover Spirit. Uncertainties quoted are standard deviations (2σ).”

“

HIGHLIGHTS:

Analysis of the mineral products of biogenic transformations of ferrihydrite to magnetite by the Fe(III)-reducing bacteria *Geobacter sulfurreducens* using the lab based MIMOS II from NASA-MER Mission.

A complete XRD and Raman mineralogical characterization has been carried on the different bio-mineralization processes for complementing the research.

The use of Mössbauer spectroscopy in combination with XRD and Raman spectroscopy presents an interesting combined system for the search of life, especially those focused on Martian mission.

1 **Abiotic versus biotic iron mineral transformation studied by a miniaturized**
2 **backscattering Mössbauer spectrometer (MIMOS II), X-ray diffraction and Raman**
3 **spectroscopy**

4 C. Markovski¹, J. M. Byrne², E. Lalla^{3,4*}, A. D. Lozano-Gorrín⁵, G. Klingelhöfer¹, F. Rull⁶,
5 A. Kappler², T. Hoffmann¹ and C. Schröder⁷

6 ¹Institut für Anorganische Chemie und Analytische Chemie, Johannes Gutenberg Universität
7 Mainz, Staudinger Weg 9, 55128 Mainz, Germany.

8 ²Geomicrobiology, Center for Applied Geoscience, Eberhard Karls Universität Tübingen,
9 Sigwartstrasse 10, 72076 Tübingen, Germany.

10 ³Centre for research in earth and space science, York University, Petrie Science Building,
11 4700 Keele St, Toronto, M3J 1P3, Ontario, Canada.

12 ⁴Austrian Space Forum, Sillufer 3a, Innsbruck, 6020, Austria

13 ⁵Departamento de Física, Universidad de La Laguna, 38200 San Cristóbal de La Laguna,
14 Santa Cruz de Tenerife, Spain.

15 ⁶Unidad Asociada UVa-CSIC a través del Centro de Astrobiología Edificio INDITI, Parque
16 Tecnológico de Boecillo, Parcela 203, E-47151 Boecillo (Valladolid), Spain.

17 ⁷Biological and Environmental Sciences, Faculty of Natural Sciences, University of Stirling,
18 Stirling FK9 4LA, Scotland, UK.

19

20 *Corresponding author: elalla@yorku.ca

21 **Abstract**

22 Searching for biomarkers or signatures of microbial transformations of minerals is a critical
23 aspect for determining how life evolved on Earth, and whether or not life may have existed
24 in other planets, including Mars. In order to solve such questions, several missions to Mars
25 have sought to determine the geochemistry and mineralogy on the Martian surface. This
26 research includes the two miniaturized Mössbauer spectrometers (MIMOS II) on board the
27 Mars Exploration Rovers Spirit and Opportunity, which have detected a variety of iron
28 minerals on Mars, including magnetite ($\text{Fe}^{2+}\text{Fe}^{3+}_2\text{O}_4$) and goethite ($\alpha\text{-FeO(OH)}$). On Earth,
29 both minerals can derive from microbiological activity (e.g. through dissimilatory iron
30 reduction of ferrihydrite by Fe(III)-reducing bacteria). Here we used a lab based MIMOS II
31 to characterize the mineral products of biogenic transformations of ferrihydrite to magnetite
32 by the Fe(III)-reducing bacteria *Geobacter sulfurreducens*. In combination with Raman
33 spectroscopy and X-ray diffraction (XRD), we observed the formation of magnetite, goethite
34 and siderite. We compared the material produced by biogenic transformations to abiotic
35 samples in order to distinguish abiotic and biotic iron minerals by techniques that are or will
36 be available onboard Martian based laboratories. The results showed the possibility to
37 distinguish the abiotic and biotic origin of the minerals. Mossbauer was able to distinguish
38 the biotic/abiotic magnetite with the interpretation of the geological context (Fe content
39 mineral assemblages and accompanying minerals) and the estimation of the particle size in a
40 non-destructive way. The Raman was able to confirm the biotic/abiotic principal peaks of the
41 magnetite, as well as the organic principal vibration bands attributed to the bacteria. Finally,
42 the XRD confirmed the particle size and mineralogy

43 **Keywords:** Bio-magnetite, Mössbauer spectroscopy, Raman spectroscopy, iron oxides.

44 **Introduction**

45 The iron redox cycle is a significant process that takes place in most environments on Earth,
46 which can be conducted by both abiotic and microbial processes. In anoxic, pH-neutral
47 environments, microbial Fe(II)-oxidation is driven by either nitrate reducing bacteria (e.g.
48 *Acidovorax* sp. BoFeN1), photoferrotrophic bacteria (e.g. *Rhodopseudomonas palustris*
49 strain TIE-1) or neutrophilic microaerophilic bacteria (e.g. *Gallionella leptothrix*) (Kappler
50 et al., 2005; Kappler and Newman, 2004; Kappler and Straub, 2005). The other half of the
51 Fe cycle is driven by microbial Fe(III) reduction, either intracellularly by magnetotactic
52 bacteria (Blakemore, 1975) or outside of the cell wall by dissimilatory iron reducing bacteria
53 (DIRB) such as *Shewanella oneidensis* and *Geobacter sulfurreducens* (Lovley and Phillips,
54 1988, 1986). DIRB combine the oxidation of an organic substrate (e.g. acetate or lactate) or
55 hydrogen with the reduction of poorly crystalline, short range ordered, Fe(III) minerals (e.g.
56 ferrihydrite ($\text{Fe}^{3+}_2\text{O}_3 \cdot 0.5\text{H}_2\text{O}$)) and can lead to the formation of many different iron mineral
57 phases and compounds including goethite, magnetite, green rust and siderite (FeCO_3) (Byrne
58 et al., 2011). The mineralogical composition of these products of reduction depends on
59 geochemical parameters, including Fe(III) reduction rate, pH, temperature and the presence
60 of electron shuttles (e.g. riboflavin, quinones and humic acids) (O'Loughlin et al., 2010;
61 Piepenbrock et al., 2011). Furthermore, a recent study suggests that magnetite can act as both
62 an electron donor and an electron acceptor to different types of Fe metabolizers depending
63 on the redox conditions (Byrne et al., 2015). In this regard, understanding the mineralogical
64 products of biomineralization processes can help to detect signatures of microbial
65 interactions with fluid, rocks, mineral deposits and subsequent diagenesis.

66 Several terrestrial environments where microbially driven Fe(III) reduction processes
67 occur (Léveillé, 2009; Rothschild and Mancinelli, 2001) have been identified, such as Rio
68 Tinto (SW Spain), Western Australian salt lake sediments (SW, Australia) and Ten Graben
69 fault system of Green River (Utah, USA), have been proposed as terrestrial analogues to the
70 types of conditions on Mars where iron cycling could have taken place (Nixon et al., 2012;
71 Ruecker et al., 2016). These terrestrial analog systems allude to the existence of Fe(III)-
72 oxyhydroxide bio-signatures and fossilized microorganisms, with Fe(III)-oxyhydroxides
73 susceptible to recrystallization to more stable forms (Léveillé, 2009; Nixon et al., 2012;
74 Parenteau et al., 2014; Ruecker et al., 2016). Utilizing Laboratory studies and natural
75 analogues can be used to help identify bio-signatures preserved from the past (NASA's Mars
76 Exploration Rover Mission *Spirit*), current (NASA's Mars Exploration Rover Mission
77 *Opportunity*; Mars Science Laboratory (MSL) *Curiosity*) or future Mars missions (ESA-
78 ExoMars rover; NASA Mars 2020) (Bish et al., 2013; Bost et al., 2015).

79 One of the most important techniques for characterizing Fe minerals on Mars is ⁵⁷Fe
80 Mössbauer spectroscopy. This technique is capable of determining the oxidation state of iron,
81 as well the mineralogy and the magnetic structure of different Fe mineral phases (Helgason,
82 2004). Indeed, two miniaturized Mössbauer spectrometers (MIMOS II) were part of the suite
83 of analytical instruments carried on board the two Mars rovers Spirit and Opportunity, which
84 landed on January 4, 2004 and January 25, 2004, respectively (Klingelhöfer et al. 2003). The
85 data collected by these vehicles have provided a significant insight into the mineralogy of
86 iron compounds on the Martian surface (Klingelhöfer et al., 2004, 2003, Morris et al., 2010,
87 2006, 2004). Raman and X-ray diffraction (XRD) techniques are among the payload of other
88 current and future space missions (Bish et al., 2013; Bost et al., 2015, 2013). This includes

89 the CheMin XRD system on the NASA MSL Curiosity mission (Bish et al., 2013) and Raman
90 instruments such as the SHERLOC (Scanning Habitable Environment with Luminescence for
91 Organics and Chemical Instrument) system, the Raman SuperCam that were selected for the
92 NASA Mars 2020 rover, and the Raman Laser Spectrometer (RLS) of the ESA ExoMars
93 rover (Grossman, 2013; Hutchinson et al., 2014; Léveillé, 2009; Wang et al., 2015).

94 In this study, we investigated the formation of biogenic magnetite nanoparticles
95 through microbial Fe(III)-reduction by the DIRB *Geobacter sulfurreducens* in the presence
96 and absence of the electron shuttling compound Anthraquinone-2,6-disulfonate (AQDS).
97 The presence of the electron shuttle is expected to greatly increase the speed of microbial
98 Fe(III)-reduction compared to experiments in which it is not present. The presence/absence
99 of AQDS should therefore have an impact on the type of mineral phases which are produced
100 during the reduction and affect their stoichiometry (i.e. Fe(II)/Fe(III) ratio). The
101 spectroscopic and mineralogical characteristics of these minerals were compared to those of
102 minerals formed from abiotic syntheses in laboratory and to natural samples. The main goal
103 of this study is to distinguish between iron minerals formed through abiotic and biotic process
104 by techniques that are or will be available onboard Martian based laboratories. In most cases,
105 Mössbauer spectroscopy can only be applied to dry powdered materials or embedded in a
106 solid matrix such as in ice or on a filter. Here, however, we use the MIMOS II instrument to
107 analyze in situ, a solid material that has deposited from an aqueous suspension. Our study is
108 analogous to experiments conducted by Zegeye et al. (2010) who performed *in situ*
109 monitoring of lepidocrocite bioreduction and magnetite formation by backscattering
110 Mössbauer spectroscopy (Zegeye et al., 2011, 2010).

111

112 **Experimental setup**

113 *Preparation of ^{57}Fe enriched Fe(III)-oxyhydroxide*

114 A starting precipitate of ^{57}Fe enriched (~12%) Fe(III)-(oxyhydr)oxide was prepared to
115 enhance the signal-to-noise ratio of the Mössbauer spectrum obtained for sediment in water.
116 Powdered naturally abundant isotope $^{56}\text{Fe}(0)$ and pure $^{57}\text{Fe}(0)$ were separately dissolved in
117 0.7 M anoxic HCl in an anoxic glovebox (MBRAUN, 100% N_2 atmosphere) and
118 continuously stirred overnight at 400 rpm leading to the formation of $^{56}\text{Fe}^{2+}$ and $^{57}\text{Fe}^{2+}$,
119 respectively. The two solutions were filtered (0.22 μm syringe tip filter) to remove any solid
120 precipitates, then mixed in a volume ratio of 10% ^{57}Fe and 90% ^{56}Fe and removed from the
121 glovebox. The ^{57}Fe (i.e. containing ~12% ^{57}Fe) enriched solution was oxidized using 400 μl
122 H_2O_2 (37%) and stirred at 400 rpm for 2 hours to form an aqueous solution of acidified Fe^{3+} .
123 KOH (5 M) was added dropwise to the Fe^{3+} solution, leading to the precipitation of the
124 Fe(III)-oxyhydroxide, at a final pH=7. The precipitate was washed of additional ions by
125 centrifugation (4000 rpm, 20 min) three times, with the supernatant discarded and the
126 precipitate re-suspended in ultrapure H_2O . After the final centrifugation step, the material
127 was kept in liquid suspension and put into a 20 ml headspace vial. The suspension was made
128 anoxic (but not dried) by applying vacuum (5 min) followed by flushing with N_2 gas (30
129 seconds), with both steps repeated three times. The final concentration of iron in the Fe(III)-
130 oxyhydroxide suspension was determined using the ferrozine assay (Stookey, 1970) to be
131 421 mmol l^{-1} .

132 *Fe(III)-reduction experiments*

133 Two separate experiments were carried out using the ferrihydrite at different times, with one
134 in 2013 and the second in 2014. For both sets of experiments, *Geobacter sulfurreducens*
135 bacteria were grown until the late log phase in basal medium (Ehrenreich and Widdel, 1994),
136 containing 25 mM acetate (electron donor), 40 mM fumarate (electron acceptor) and buffered
137 with 22 mM NaHCO₃. The bacteria were then centrifuged three times (4000 rpm; 20 min) to
138 remove the growth medium and washed with 30 mM NaHCO₃ in between centrifugation
139 steps. The final cell suspension was made up to a volume of 2 ml and the optical density at λ
140 = 600 nm (OD₆₀₀) measured at 0.385 abs and 0.372 abs (FlashScan 550, Analytik Jena,
141 Germany) for experiments in 2013 and 2014 respectively.

142 All Fe(III) reduction experiments were prepared in Plexiglas holders with a 500 μ m bottom
143 thickness. For 2013 experiments, cultures were prepared up to a volume of 15 ml in the
144 glovebox using sterile, anoxic solutions and consisted of 50 mmol L⁻¹ Fe(III)-
145 (oxyhydr)oxide, 20 mM acetate and 30 mM NaHCO₃. One of the cultures additionally
146 contained AQDS (10 μ M) as an electron shuttle. Both culture experiments were sealed with
147 a rubber butyl stopper to maintain an anoxic environment. The culture experiments were
148 inoculated with 0.312 ml of *G. sulfurreducens* cell suspension immediately prior to loading
149 on to the MIMOS II device. The cultures are subsequently referred to as FH+AQDS-13 and
150 FH-AQDS-13.

151 For the 2014 experiment, the culture were prepared in a similar way, however it contained
152 double the concentration of iron material, i.e. 100 mmol L⁻¹ Fe(III)-oxyhydroxide, 40 mM
153 acetate and 30 mM NaHCO₃. There was no AQDS present. The 2014 experiment was
154 inoculated with 0.644 ml of the *G. sulfurreducens* cell suspension, so approximately twice
155 as many cells as for the 2013 experiment. This culture is referred hereafter as FH-AQDS-14.

156 *Analytical methods*

157 During the 2014 experiments, *in situ* Mössbauer measurements were carried out throughout
158 the course of the experiment on each samples and it preparation. These *in situ* Mössbauer
159 spectra were collected by placing the culture incubation vessels onto a MIMOS II in
160 backscattering geometry at the Mössbauer Group of Mainz University (Germany) and left
161 for the duration of the experiment. The culture vessels during the 2013 experiments were
162 left on the MIMOS II, however the recorded spectra were not of sufficient quality due to their
163 lower iron concentrations. Following the reduction phase of each experiment, the contents of
164 each of the reaction vessels were filtered with Millipore swinnex filter holders and Millipore
165 membrane filters (0.45 μm - HAWP04700). The entire solution of these experiments were
166 passed through the filter and then dried under an N_2 atmosphere. Filtered samples were sealed
167 in between two layers of Kapton tape to inhibit oxidation of the samples during measurement,
168 and Mössbauer spectra were collected with the MIMOS II instrument. Spectra were
169 calibrated against alpha-iron at room temperature and fitted with an in house routine (Mbfite)
170 using Lorentzian and Voigt line profiles. Mbfite is based on the least-squares minimization
171 routine MINUIT (James, 2004). All Mössbauer fitting parameters are shown in Table 1 (i.e.
172 center shift (CS), quadrupole splitting (ΔE_Q), hyperfine field (B_{hf})).

173 Dried samples from the 2013 experiments (i.e. FH-AQDS-13 and FH+AQDS-13) were
174 analyzed using X-ray diffraction (XRD), with data collected using a Bruker D8 Discovery
175 Diffractometer equipped with a molybdenum $K_{\alpha 1}$ X-ray tube ($\lambda = 0.71 \text{ \AA}$) at the Institut für
176 Anorganische Chemie und Analytische Chemie of Mainz University (Germany). Total
177 scattering was measured between 5° and $40^\circ 2\theta$. A comparison with a natural rock magnetite
178 standard has been done. The natural magnetite used belongs to the NASA Athena Reference

179 Samples (Aref 043) (Schröder, 2003). Magnetite sample was ground in an agate mortar and
180 fixed onto a polymer tape (Scotch). The data were refined using the Rietveld method
181 (Rietveld, 1969) and the FULLPROF software (Rodríguez-Carvajal, 1993). A pseudo-Voigt
182 function was used to describe the peak shape and a polynomial function with five refinement
183 coefficients for the background.

184 Spectroscopic Raman measurement were performed at the Unidad Asociada Uva-CSIC
185 (Valladolid, Spain) on the dried samples from the 2013 experiments (i.e. FH-AQDS-13 and
186 FH+AQDS-13). The Raman mineralogical characterization of the sample was performed by
187 micro-Raman spectroscopy, using a microscope Nikon Eclipse E600 coupled to a
188 spectrometer KOSI Holospec f/1.8i with a resolution of 5 cm^{-1} illuminated by a laser REO
189 LSRP-3501, He-Ne 632.8 nm. The detection was performed by a CCD Andor DV420A-OE-
190 130 with a resolution of 5 cm^{-1} . The laser power used is 14 mW with a spot diameter of 15
191 μm . The kapton cover of prepared samples produce strong Raman fluorescence. The material
192 was carefully extracted from the Plexiglas holders inside a chamber/bell with a nitrogen
193 atmosphere to avoid abiotic oxidation. Moreover, some natural iron-oxides, sulfate and
194 carbonate from the sample collection of the ESA-ExoMars Raman Laser Spectrometer (RLS)
195 database were measured and used as a reference materials. The reference samples stem (1)
196 from several fieldtrips to terrestrial analogues including Rio Tinto (Spain), Tenerife (Spain),
197 Svalbard (Norway), Faroe Island, etc. (Lalla et al., 2016, 2015; Sansano et al., 2015) or (2)
198 were synthesized in the laboratory (Sansano-Caramazana, 2015). The spectral Raman
199 collection of the mineral phases has been obtained using standard Raman systems and the
200 RLS simulator system, processed and analyzed using the protocols for the ExoMars mission
201 (Hermosilla et al., 2012).

202 **Results**

203 ***Mössbauer analysis***

204 Data were obtained for the FH-AQDS-14 experiment which was incubated at room
205 temperature on a MIMOS II throughout the microbial Fe(III) reduction over the course of 19
206 days (Figure 1a and b) and are consequently referred to as *in situ* measurements. Figure 1a
207 shows the recorded spectrum obtained for FH-AQDS-14 after 6 h, with a clear doublet visible
208 despite the fact that the starting precipitate (ferrihydrite) is suspended in liquid media. Figure
209 1b shows the recorded spectrum for FH-AQDS-14 after 19 days of incubation on the MIMOS
210 II, with the data clearly indicating the presence of both a doublet and sextet. After 19 days
211 the microbial Fe(III) reduction in the *in situ* experiments was stopped and the precipitates
212 were filtered. The filtered samples were then placed onto the MIMOS II again for further
213 analysis, with Figure 1c showing the spectrum from the FH-AQDS-14 filtered sample at
214 room temperature. It is clear from the figure that after 6 h, the sample displays a spectrum
215 corresponding to ferrihydrite, whilst after 19 days, the sample shows a clear sextet which
216 likely corresponds to magnetite. After filtration (Figure 1c), the sample displays a more
217 characteristic spectrum of magnetite, though additional peaks corresponding to ferrihydrite
218 and goethite appear to be present.

219 Figure 2 shows the data collected for FH-AQDS-13 (Figure 2a) and FH+AQDS-13 (Figure
220 2b) experiments measured at room temperature after filtration and loaded directly onto the
221 MIMOS II instrument. The Mössbauer spectra for a reference sample of magnetite (Athena
222 Reference Sample 043) is shown in Figure 2c for comparison and clearly shows the
223 tetrahedral and octahedral lattice sites expected for the mineral. Figure 2 indicates that
224 ferrihydrite FH-AQDS-13 was transformed mainly into pure magnetite, whilst
225 FH+AQDS-13 was transformed to magnetite, but with traces of siderite.

226 ***XRD***

227 XRD data shown in Figure 3 confirms that the only mineral phase present in sample FH-
228 AQDS-13 at the end of the experiment was magnetite whereas sample FH+AQDS-13
229 contained both magnetite and siderite, confirming the Mössbauer results. The structure of
230 magnetite is centrosymmetric and shows cubic symmetry with space group $Fd-3m$. The
231 lattice parameter for FH-AQDS-13 and the FH+AQDS-13 samples show values around 8.30
232 Å which is comparable to known standards. The average crystallite sizes for both samples
233 (also known as the coherent scattering domain) has been determined through the use of the
234 Scherrer equation (Scherrer, 1918), being around 27-30 nm.

235 ***Raman analysis***

236 Raman spectroscopy was carried out on selected areas of samples FH+AQDS-13 and FH-
237 AQDS-13 (Figure 4) and compared to reference bands for several different iron minerals
238 (Table 2) (Hanesch, 2009). The measured data has been processed by a Gaussian curve fitting
239 analysis on each band to obtain the correct band position of the different minerals phases on
240 the spectra. The fitting has been obtained by using the commercial program Bruker OPUS
241 and following the standard procedure: spectra smoothing (if it is needed), background
242 subtraction, normalization and interactive curve fitting (by Levenberg-Marquardt and/or
243 Local Least Squares methods).

244 The results show the existence of several mineral oxides such as hematite, magnetite, siderite,
245 and possibly poorly crystalline goethite in the band fitting (Figure 4 and Table 3). The bands
246 in the region at 120 to 220 cm^{-1} belong unambiguously to the siderite being present on the
247 different spectra. Secondly, the bands of the region 220-420 cm^{-1} have been assigned to the

248 vibration of hematite (~ 225 , ~ 245 , ~ 290 cm^{-1}), siderite (~ 287 cm^{-1}), goethite (~ 244 , ~ 300
249 and ~ 385 cm^{-1}) and magnetite (310 cm^{-1}). However, the bands corresponding to
250 FH-AQDS-13 (Figure 4a and 4b) are more intense compared to FH+AQDS-13 (Figure 4c
251 and 4d) due to the influence of goethite presenting the strongest vibration in this band region
252 (according to the band fitting). On the other hand, the region $420\text{-}550$ cm^{-1} presents the
253 vibration of goethite (~ 480 cm^{-1}), magnetite (~ 530 cm^{-1}), hematite (~ 500 cm^{-1}) and siderite
254 (~ 500 cm^{-1}). The bands on FH-AQDS-13 obtained by the curve fitting show a strong
255 influence caused by amorphous goethite (Figure 4a and 4b).

256 The region from 560 to 800 cm^{-1} can be assigned mainly to the magnetite (~ 650 cm^{-1}),
257 possibly goethite (681 cm^{-1}), hematite (~ 610 and ~ 660 cm^{-1}) and siderite (~ 720 cm^{-1}). Finally,
258 the region within the $1200\text{-}1650$ cm^{-1} presents a mixture of bands that belong to
259 hematite/goethite magnon (~ 1350 cm^{-1}) and organics (~ 1314 , ~ 1422 , ~ 1545 and ~ 1575 cm^{-1}).
260

261 The magnetite bands are clearly visible at 300 , 532 and 661 cm^{-1} which are in close agreement
262 with other studies (Hanesch, 2009; Shebanova and Lazor, 2003). The intense bands
263 corresponding to the A_{1g} mode at 667 cm^{-1} presents a variation of magnetite measured in other
264 studies. The A_{1g} oxide peak of magnetite is shifted toward higher wave numbers in the bio-
265 magnetite (700 cm^{-1}) compared to that of the inorganically produced magnetite (670 cm^{-1})
266 (Jimenez-Lopez et al., 2010). In previous studies, it has been found that a transition to an
267 orthorhombic phase on a starting oxidation process produces a displacement of the A_{1g} to
268 higher values (Shebanova and Lazor, 2003). The second magnetite band between 532 and
269 550 cm^{-1} is reported as the mode F_{2g} and is observed to be sensitive to possible defects in the
270 crystal structure as well as the presence of vacancies and interstitial cations. Furthermore,

271 other studies suggest that the F_{2g} band below to 500 cm^{-1} can be attributed to the occurrence
272 of hematite (de Faria et al., 1997; Hanesch, 2009; Shebanova and Lazor, 2003). The siderite
273 presents the strongest band at 182, 287, 731 and 1090 cm^{-1} (Hanesch, 2009; Rull et al., 2004).
274 The band fitting also reveals the existence of hematite and it presents as a combination of
275 several vibrations at 225, 245, 291, 410, 500 and 611 cm^{-1} with the magnon at 1321 cm^{-1}
276 (Hanesch, 2009). In the case of the possible goethite presence, the principal vibrations are at
277 244, 299, 385, 480 and 681 cm^{-1} being the most commonly used for the identification in
278 complex vibrational analysis (de Faria et al., 1997; Hanesch, 2009; Rull et al., 2004). The
279 bands at the aforementioned positions are very weak and broadened, due to poorly
280 crystallized goethite, which is combined with other oxide mineral phases (magnetite and
281 hematite).

282 When considering the Raman bands of biological component, the most intense vibrations
283 were detected between 1300 and 1600 cm^{-1} , which can be assigned to the active modes D
284 and G of the C-C bonds vibrations from carbonaceous materials. The band fitting
285 corresponding to this vibrational region presents several medium intensity vibrations at 1314,
286 1422 and 1565 cm^{-1} according to the best fitting analysis. The bands at 1314 and 1422 cm^{-1}
287 can be assigned to the D double modes D1 and D2, which is in agreement with other studies
288 (Ferrari, 2007). However, it has been found during band fitting that an influence of other
289 magnon vibrations of hematite/goethite phases on 1350 cm^{-1} (Hanesch, 2009; Rull et al.,
290 2007) is possible. The band G has also been observed (see Table 3), showing a distorted
291 structure clearly detectable by the broad bands. The vibrations at 2903 and 2961 cm^{-1}
292 correspond to the C-H vibrational regions, which could be assigned to symmetric and
293 asymmetric stretching of the $-\text{CH}_3$ from the organic matter (Böttger et al., 2012; Pereira et

294 al., 2007). Furthermore, the *G. sulfurreducens* Raman vibration bands can be assigned to the
295 peaks detected along the different spectra measurements. In this regard, several vibrations
296 have been identified considering the following regions: (1) the C-H stretching region bands
297 on 2900-3000 cm⁻¹; (2) the CH deformation vibrational region between 1300 and 1450 cm⁻¹;
298 and (3) the C=O stretching vibration zone in 1650 to 1800 cm⁻¹ approximately (el-Kabbani
299 et al., 1991; Kudelski, 2005).

300 **Discussion**

301 The *in situ* Mössbauer spectrum for FH-AQDS-14 after 6 h is dominated by the presence of
302 a doublet corresponding to ferrihydrite. After 19 days the sample is still dominated by a
303 central ferric doublet, although a sextet is clearly evident. In the filtered sample however
304 (Figure 1c), it is clear that the Mössbauer spectrum displays two sextets corresponding to (1)
305 tetrahedrally coordinated iron denoted Fe³⁺_{tet}, and (2) octahedrally coordinated Fe which
306 includes both Fe²⁺ and Fe³⁺, often denoted Fe^{2.5+}_{oct} with an additional goethite phase. This
307 apparent difference in the sample before and after filtration is likely due to the nature of the
308 MIMOS II instrument, with the *in situ* experiments only looking at the very bottom layer of
309 the iron layer which was undergoing microbial transformation. A gradient in the reaction
310 likely existed with most reduction taking place in the top portion of the sample where the
311 mineral is more exposed to the solution (Dippon et al., 2015). When the sample was filtered,
312 it was mixed and so the top fraction and bottom fraction were mixed and thus yielded the
313 sextet as seen in Figure 1c. The goethite phase present in the filtered sample of FH-AQDS-14
314 was fitted with a sextet in which the hyperfine magnetic field (B_{hf}) value (Table 1) is smaller
315 than that of well-crystalline goethite, indicating that the goethite has very low crystallinity or
316 consists of very small particles.

317 In the experiments carried out in 2013, sample FH-AQDS-13 (Figure 2a) appears to have
318 more well-defined sextets than sample FH+AQDS-13 (Figure 2b). The broadened lines and
319 additional broad sextet in these spectra can be explained by a lower degree of crystallinity
320 possibly because of impurities in the magnetite structure, e.g. the incorporation of organic
321 matter, and/or small particle sizes. In magnetically ordered phases, which present as sextets
322 in Mössbauer spectra, these influences reduce the strength of the internal B_{hf} . A range of
323 degrees of crystallinity then results in broad lines skewed towards smaller B_{hf} values. Small
324 particle sizes, generally 30 nm or less, can additionally lead to an effect called
325 superparamagnetism (Daniels and Rosencwaig, 1969). The particle sizes are then in the range
326 of individual magnetic domains and random thermal movement of the particles leads to a net
327 zero magnetic field and magnetic ordering appears to collapse, which manifests itself as a
328 paramagnetic doublet in the Mössbauer spectrum instead of a magnetically ordered sextet
329 (Daniels and Rosencwaig, 1969; Dezsi et al., 2008). Superparamagnetism appears to be
330 visible in sample FH+AQDS-13 with the very broad lines in the Mössbauer spectrum (Figure
331 2b) in agreement with previous studies which have shown the samples prepared in the
332 presence of electron shuttles (e.g. AQDS) tend to be smaller in diameter than those without
333 (Byrne et al., 2011). Furthermore, the FH+AQDS-13 sample clearly contains siderite which
334 is likely due to the enhanced rate of microbially driven Fe(III) reduction, due to the presence
335 of AQDS, resulting in an excess of Fe^{2+} in solution which can further react with the CO_3^{2-}
336 present in solution from the buffer system and lead to the precipitation of siderite (Cornell
337 and Schwertmann, 2003; Hansel et al., 2003; Liu et al., 2009).

338 The parameters obtained from fitting the magnetite spectra closely correspond to the values
339 expected for magnetite (Table 1). All of the hyperfine parameters determined are in general

340 smaller than expected, however this is likely due to the sample exhibiting poorer magnetic
341 ordering at room temperature than well-crystalline, stoichiometric magnetite (Figure 2c).
342 Neglecting potential differences in f -factor for the different Fe lattice positions, the
343 stoichiometric ratio ($x=\text{Fe(II)}/\text{Fe(III)}$) of magnetite can be determined by comparing the
344 relative areas of the two sextets according to the following equation (Da Costa et al., 1995;
345 Daniels and Rosencwaig, 1969):

$$346 \quad x = \frac{0.5 Fe_{oct}^{2.5+}}{0.5 Fe_{oct}^{2.5+} + Fe_{tet}^{3+}} \quad (1)$$

347 Using equation 1 it is seen that magnetite formed in FH+AQDS-13 ($x = 0.25$) is more
348 oxidized than perfectly stoichiometric magnetite ($x = 0.5$). The iron in magnetite formed in
349 FH-AQDS-13 ($x = 0.65$) is more reduced than stoichiometric magnetite. The difference is
350 thought to be due to the faster reduction rate in the presence of AQDS, leading to the
351 formation of superparamagnetic magnetite nanoparticles. However, this result also suggests
352 that the presence of electron shuttles might in fact lead to the formation of rather oxidized
353 magnetite. Since electron shuttles such as AQDS are organic compound, it might indicate
354 that magnetite found in regions with low stoichiometry can be linked to the presence of
355 organic substance. The relative ratio of Fe(II)/Fe(III) in the magnetite in FH-AQDS-13 is
356 calculated to be higher than those previously reported and showing a higher concentration
357 of ferrous magnetite (Veeramani et al., 2011). Moreover, the mineral phases measured are in
358 agreement with Veeramani *et al.*, (Veeramani et al., 2011), though here we have also
359 identified the presence of siderite.

360 The XRD results for our samples show smaller values for the lattice constant(8.30 Å) than
361 the 8.397 Å associated with stoichiometric magnetite (ICDD, n.d.; “Magnetite -

362 www.mindat.org,” 2001). Maghemite has a smaller lattice constant of 8.33 Å, which is more
363 similar to our results, suggesting the samples to be partially oxidized which agrees with the
364 Mössbauer results for sample FH+AQDS (Wohlfarth and Arrott, 1982). It has also been seen
365 that the lattice parameters of pure and metal-substituted bio-magnetites tend to be smaller
366 compared to those of chem-magnetites where the bio-magnetite likely has a relatively more
367 compact crystal structure with fewer uncoordinated iron ions on the surface (Moon et al.,
368 2010). The average crystal size is around 27-30 nm for the FH+AQDS-13 and FH-AQDS-13,
369 being consistent with the Mössbauer observations of smaller B_{hf} values, broadened and
370 skewed lines, and superparamagnetism. Also, this result confirms the interpretation of other
371 studies (Byrne et al., 2011; Veeramani et al., 2011).

372 In the Raman results, the variation of A_{1g} mode corresponding to the magnetite could
373 be caused by the curve fitting or may be due to structural changes generated during the
374 microbial Fe(III) reduction where the oxidation process produces a displacement of the A_{1g}
375 to higher values. An estimation can be done by curve fitting relative band intensity of I_{685-90}
376 $/I_{650}$ produced by the magnetite and the bio-magnetite, the results show the existence of two
377 Raman bands where the I_{685-90} is more intense (See Table 3b – Figure 3). Also, the
378 FH-AQDS-13 presents the possible existence of goethite due to the higher intensity of the
379 bands in the region between 220-420. Furthermore, it can be affirmed by the $I_{220-520}/I_{560-800}$,
380 which for FH-AQDS-13 is at approximately 0.5 and FH+AQDS-13 is 0.35 (Figure 3).

381 In the region from 2800 to 3100 cm^{-1} , the FH-AQDS-13 bands are more intense compared to
382 those of FH+AQDS-13 spectra and confirm that the *G. sulfurreducens* transformed the
383 starting material.

384 In general, the combination of Mössbauer, Raman and XRD technique allowed the detection
385 of several iron mineral phases and mineral structures. The magnetite was the main mineral
386 that formed as a result of microbial Fe(III) reduction by *G. sulfurreducens*. The Raman based
387 vibrational technique was able to detect hematite with the possibility of minor phases of
388 goethite, clearly distinguishable by the main vibrations and the curve-fitting. Mössbauer
389 spectra indicate oxidized magnetite in the FH+AQDS-13 samples. Oxidation of magnetite
390 leads to maghemite and eventually hematite formation, but these phases are difficult to
391 differentiate (Vandenberghe et al., 2000).

392 The combination of siderite, magnetite, hematite and non-crystalline goethite suggests a
393 relatively complex mineralization process that is strongly dependent on biological
394 mechanism. Similar formations of mixed minerals can be achieved by chemical processes,
395 however they often present with other phase combinations including ferrihydrite-goethite-
396 lepidocrocite-magnetite (Hansel et al., 2005) or goethite-hematite-maghemite-magnetite-
397 akaganeite (Ahn et al., 2012). Furthermore, the starting conditions of microbial Fe(III)
398 reduction, such as the use of different starting substrates including hydrous ferric oxide,
399 goethite, hematite, magnetite, carbonates, and Fe(III)-clays, or the variation of geochemical
400 parameters including Eh, pH, and temperature can yield stark differences in the types of
401 minerals produced via primary or secondary mineralization pathways (Jimenez-Lopez et al.,
402 2010; Perez-Gonzalez et al., 2010).

403 Here we suggest that the use of Mössbauer-Raman-XRD analyses in combination with other
404 structural studies could potentially be used to obtain a suitable range of criteria to help
405 develop fingerprints to distinguish biological and abiotic magnetite. The biogenic magnetite
406 and goethite from our experiments differs significantly from the magnetite and goethite

407 observed with the Mars Exploration Rovers in rocks and soils on Mars (Table 1), where the
408 magnetite is suggested to be of primary, igneous origin (Morris et al., 2008).

409 Our biogenic magnetite is non-stoichiometric and, in the case of FH+AQDS-13 appears to
410 be oxidized. The broad lines reflect in Mössbauer spectra reflect low crystallinity, potentially
411 resulting from impurities such as organic matter, and/or small particle sizes. The presence of
412 organic matter is confirmed by Raman spectroscopy and small particle sizes are indicated by
413 XRD. Taken together, the evidence extracted from the different techniques could be used to
414 establish some criteria for bio-signatures. Table 4 presents a resume of the main features of
415 each technique that could be used for the detection of bio-signatures in planetary exploration.

416 The question, however, is whether the features observed here would be preserved over
417 geological timescales. Over time, magnetite might mature and increase in crystallinity while
418 organic matter can undergo decay, thus potentially eliminating any evidence over extended
419 timescales.

420 **Conclusions**

421 The MIMOS II instrument, of which two have previously been sent to Mars onboard Martian
422 rovers, has been used to characterize different mineral phases produced by the microbial
423 reduction of Fe(III)-oxyhydroxide and determined the dominant phase produced to be
424 magnetite. Other techniques on current or future Mars rover missions such as XRD and
425 Raman have been used to complement these results. Mössbauer, XRD, and Raman confirm
426 the existence of magnetite for the samples incubated with only ferrihydrite (FH+AQDS-13
427 and FH-AQDS-13) and magnetite combined with siderite for the sample incubated with an
428 added electron shuttle (FH+AQDS-13). The values of the crystal lattice show values under

429 8.397 Å and crystalline sizes under 30 nm being in the range of superparamagnetism as
430 confirmed by the Mössbauer analysis.

431 Raman analysis shows the formation of different mineralization products, including goethite
432 (possibly), hematite, magnetite and siderite which is only somewhat in agreement with the
433 Mössbauer analyses that did not observe hematite in samples. Some differences between the
434 bio-magnetite and natural magnetite have been detected by Raman spectroscopy on the bands
435 at approximately 650 and 540 cm⁻¹. In all spectra recorded, organic compounds were detected
436 which correspond to the DIRB *G. sulfurreducens*.

437 The combination of these three different analytical techniques could be used as a critical
438 approach for observing the products of Fe-biomineralization processes on future space
439 missions, especially those focused on Mars. In this regard, these techniques, used in
440 combination with morphological studies, will help to establish a criterion of the biological
441 origin of biogenic magnetite and other Fe minerals.

442 **Acknowledgements**

443 The work was supported by the MICINN with the Project AYA-2008-04529 for the
444 development of the Raman-LIBS combined spectrometer for the ESA-ExoMars Mission. C.
445 S. acknowledges a joint postdoctoral appointment at the Universities of Bayreuth and
446 Tübingen funded through the DFG research unit FOR 580 – electron transfer processes in
447 anoxic aquifers (e-TraP) and an Impact Fellowship awarded by the University of Stirling.
448 Finally, the authors would like to thank the anonymous reviewers for their helpful and
449 constructive comments that greatly contributed to improving the final version of the paper.

450 **References**

451 Ahn, T., Kim, J.H., Yang, H.M., Lee, J.W., Kim, J.D., 2012. Formation pathways of
452 magnetite nanoparticles by coprecipitation method. *J. Phys. Chem. C* 116, 6069–6076.
453 doi:10.1021/jp211843g

454 Bish, D.L., Blake, D.F., Vaniman, D.T., Chipera, S.J., Morris, R. V, Ming, D.W., Treiman,
455 A.H., Sarrazin, P., Morrison, S.M., Downs, R.T., Achilles, C.N., Yen, A.S., Bristow,
456 T.F., Crisp, J.A., Morookian, J.M., Farmer, J.D., Rampe, E.B., Stolper, E.M.,
457 Spanovich, N., Team, M.S.L.S., 2013. X-ray Diffraction Results from Mars Science
458 Laboratory: Mineralogy of Rocknest at Gale Crater. *Sci.* 341.
459 doi:10.1126/science.1238932

460 Blakemore, R., 1975. Magnetotactic bacteria. *Sci.* 190, 377–379.
461 doi:10.1126/science.170679

462 Bost, N., Ramboz, C., LeBreton, N., Foucher, F., Lopez-Reyes, G., De Angelis, S., Josset,
463 M., Venegas, G., Sanz-Arranz, A., Rull, F., Medina, J., Josset, J.-L., Souchon, A.,
464 Ammannito, E., De Sanctis, M.C., Di Iorio, T., Carli, C., Vago, J.L., Westall, F., 2015.
465 Testing the ability of the ExoMars 2018 payload to document geological context and
466 potential habitability on Mars. *Planet. Space Sci.* 108, 87–97.
467 doi:10.1016/j.pss.2015.01.006

468 Bost, N., Westall, F., Ramboz, C., Foucher, F., Pullan, D., Meunier, A., Petit, S., Fleischer,
469 I., Klingelhöfer, G., Vago, J.L., 2013. Missions to Mars: Characterisation of Mars
470 analogue rocks for the International Space Analogue Rockstore (ISAR). *Planet. Space*
471 *Sci.* 82–83, 113–127. doi:http://dx.doi.org/10.1016/j.pss.2013.04.006

472 Böttger, U., de Vera, J.-P., Fritz, J., Weber, I., Hübers, H.-W., Schulze-Makuch, D., 2012.

473 Optimizing the detection of carotene in cyanobacteria in a martian regolith analogue
474 with a Raman spectrometer for the ExoMars mission. *Planet. Space Sci.* 60, 356–362.
475 doi:<http://dx.doi.org/10.1016/j.pss.2011.10.017>

476 Byrne, J.M., Klueglein, N., Pearce, C., Rosso, K.M., Appel, E., Kappler, A., 2015. Redox
477 cycling of Fe(II) and Fe(III) in magnetite by Fe-metabolizing bacteria. *Science* (80-.).
478 347, 1473–1476. doi:10.1126/science.aaa4834

479 Byrne, J.M., Telling, N.D., Coker, V.S., Patrick, R.A.D., van der Laan, G., Arenholz, E.,
480 Tuna, F., Lloyd, J.R., 2011. Control of nanoparticle size, reactivity and magnetic
481 properties during the bioproduction of magnetite by *Geobacter sulfurreducens*.
482 *Nanotechnology* 22, 455709.

483 Cornell, R.M., Schwertmann, U., 2003. The iron oxides: structure, Properties, Reactions,
484 Occurrences and Uses, in: Wiley-Vch. p. ISBN: 3-527-30274-3.
485 doi:10.1002/3527602097

486 Da Costa, G.M., De Grave, E., De Bakker, P.M.A., Vandenberghe, R.E., 1995. Influence of
487 nonstoichiometry and the presence of maghemite on the Mössbauer spectrum of
488 magnetite. *Clays Clay Miner.* 43, 656–668.

489 Daniels, J.M., Rosencwaig, A., 1969. Mössbauer spectroscopy of stoichiometric and non-
490 stoichiometric magnetite. *J. Phys. Chem. Solids* 30, 1561–1571. doi:10.1016/0022-
491 3697(69)90217-0

492 de Faria, D.L.A., Silva, S.V., de Oliveira, M.T., 1997. Raman microspectroscopy of some
493 iron oxides and oxyhydroxides. *J. Raman Spectrosc.* 28, 873–878.

494 Dezső, I., Fetzter, C., Gombköt, Á., Szucs, I., Gubicza, J., Ungár, T., 2008. Phase transition

495 in nanomagnetite. *J. Appl. Phys.* 103, 1–5. doi:10.1063/1.2937252

496 Dippon, U., Schmidt, C., Behrens, S., Kappler, A., Dippon, U.R.S., Schmidt, C., Behrens,
497 S., Kappler, A., 2015. Secondary Mineral Formation During Ferrihydrite Reduction by
498 *Shewanella oneidensis* MR-1 Depends on Incubation Vessel Orientation and Resulting
499 Gradients of Cells, Fe and Fe Minerals. *Geomicrobiol. J.* 451.
500 doi:10.1080/01490451.2015.1017623

501 Ehrenreich, A., Widdel, F., 1994. Anaerobic oxidation of ferrous iron by purple bacteria, a
502 new type of phototrophic metabolism. *Appl. Environ. Microbiol.* 60, 4517–4526.

503 el-Kabbani, O., Chang, C.H., Tiede, D., Norris, J., Schiffer, M., 1991. Comparison of
504 reaction centers from *Rhodobacter sphaeroides* and *Rhodospseudomonas viridis*:
505 overall architecture and protein-pigment interactions. *Biochemistry* 30, 5361–5369.

506 Ferrari, A.C., 2007. Raman spectroscopy of graphene and graphite: Disorder, electron-
507 phonon coupling, doping and nonadiabatic effects. *Solid State Commun.* 143, 47–57.

508 Grossman, L., 2013. NASA urged to seek live Martians with 2020 rover. *New Sci.* 219, 9.
509 doi:10.1016/S0262-4079(13)61775-3

510 Hanesch, M., 2009. Raman spectroscopy of iron oxides and (oxy)hydroxides at low laser
511 power and possible applications in environmental magnetic studies. *Geophys. J. Int.*
512 177, 941–948. doi:10.1111/j.1365-246X.2009.04122.x

513 Hansel, C.M., Benner, S.G., Fendorf, S., 2005. Competing Fe (II)-induced mineralization
514 pathways of ferrihydrite. *Environ. Sci. Technol.* 39, 7147–7153.
515 doi:10.1021/es050666z

516 Hansel, C.M., Benner, S.G., Neiss, J., Dohnalkova, A., Kukkadapu, R.K., Fendorf, S.,

517 2003. Secondary mineralization pathways induced by dissimilatory iron reduction of
518 ferrihydrite under advective flow. *Geochim. Cosmochim. Acta* 67, 2977–2992.

519 Helgason, O., 2004. Processes in geophysics studied by Mossbauer spectroscopy.
520 *Hyperfine Interact.* 156, 379–388. doi:10.1023/B:HYPE.0000043257.28606.14

521 Hermosilla, I., Lopez-Reyes, G., Catala, A., Sanz, A., Llanos, D.R., Rull, F., 2012. Raman
522 spectra processing algorithms and database for RLS-ExoMars. *Proc. Eur. Planet. Sci.*
523 *Congr.* 7, 23–28.

524 Hutchinson, I.B., Parnell, J., Edwards, H.G.M., Jehlicka, J., Marshall, C.P., Harris, L. V,
525 Ingle, R., 2014. Potential for analysis of carbonaceous matter on Mars using Raman
526 spectroscopy. *Planet. Space Sci.* doi:http://dx.doi.org/10.1016/j.pss.2014.07.006

527 ICDD, n.d. PDF-2 database.

528 James, F., 2004. MINUIT Tutorial, Function Minimization, in: *CERN Computing and Data*
529 *Processing School*. Pertisau, pp. 10–24.

530 Jimenez-Lopez, C., Romanek, C.S., Bazylinski, D.A., 2010. Magnetite as a prokaryotic
531 biomarker: A review. *J. Geophys. Res.* 115, G00G03. doi:10.1029/2009JG001152

532 Kappler, A., Newman, D.K., 2004. Formation of Fe(III)-minerals by Fe(II)-oxidizing
533 photoautotrophic bacteria. *Geochim. Cosmochim. Acta* 68, 1217–1226.
534 doi:10.1016/j.gca.2003.09.006

535 Kappler, A., Schink, B., Newman, D.K., 2005. Fe(III) mineral formation and cell
536 encrustation by the nitrate-dependent Fe(II)-oxidizer strain BoFeN1. *Geobiology* 3,
537 235–245. doi:10.1111/j.1472-4669.2006.00056.x

538 Kappler, A., Straub, K.L., 2005. Geomicrobiological Cycling of Iron. *Rev. Mineral.*
539 *Geochemistry* 59, 85–108. doi:10.2138/rmg.2005.59.5

540 Klingelhöfer, G., Morris, R. V, Bernhardt, B., Rodionov, D., de Souza, P.A., Squyres,
541 S.W., Foh, J., Kankeleit, E., Bonnes, U., Gellert, R., Schröder, C., Linkin, S., Evlanov,
542 E., Zubkov, B., Prilutski, O., 2003. Athena MIMOS II Mössbauer spectrometer
543 investigation. *J. Geophys. Res. Planets* 108, n/a--n/a. doi:10.1029/2003JE002138

544 Klingelhöfer, G., Morris, R. V, Bernhardt, B., Schröder, C., Rodionov, D.S., de Souza,
545 P.A., Yen, A., Gellert, R., Evlanov, E.N., Zubkov, B., Foh, J., Bonnes, U., Kankeleit,
546 E., Gütlich, P., Ming, D.W., Renz, F., Wdowiak, T., Squyres, S.W., Arvidson, R.E.,
547 2004. Jarosite and Hematite at Meridiani Planum from Opportunity's Mössbauer
548 Spectrometer. *Sci.* 306, 1740–1745. doi:10.1126/science.1104653

549 Kudelski, A., 2005. Characterization of thiolate-based mono- and bilayers by vibrational
550 spectroscopy: A review. *Vib. Spectrosc.*

551 Lalla, E.A., López-Reyes, G., Sansano, A., Sanz-Arranz, A., Schmanke, D., Klingelhöfer,
552 G., Medina-García, J., Martínez-Frías, J., Rull-Pérez, F., 2015. Estudio
553 espectroscópico y DRX de afloramientos terrestres volcánicos en la isla de Tenerife
554 como posibles análogos de la geología marciana. *Estud. Geológicos* 71, 1–19.
555 doi:10.3989/egeol.41927.354

556 Lalla, E.A., Sanz-Arranz, A., Lopez-Reyes, G., Sansano, A., Medina, J., Schmanke, D.,
557 Klingelhoef, G., Rodríguez-Losada, J.A., Martínez-Frías, J., Rull, F., 2016. Raman–
558 Mössbauer–XRD studies of selected samples from “Los Azulejos” outcrop: A possible
559 analogue for assessing the alteration processes on Mars. *Adv. Sp. Res.* 57, 2385–2395.

560 doi:10.1016/j.asr.2016.03.014

561 L veill , R., 2009. Validation of astrobiology technologies and instrument operations in
562 terrestrial analogue environments. *Comptes Rendus Palevol* 8, 637–648.

563 doi:<http://dx.doi.org/10.1016/j.crpv.2009.03.005>

564 Liu, H., Li, P., Lu, B., Wei, Y., Sun, Y., 2009. Transformation of ferrihydrite in the
565 presence or absence of trace Fe(II): The effect of preparation procedures of
566 ferrihydrite. *J. Solid State Chem.* 182, 1767–1771.

567 Lovley, D.R., Phillips, E.J.P., 1988. Novel Mode of Microbial Energy Metabolism: Organic
568 Carbon Oxidation Coupled to Dissimilatory Reduction of Iron or Manganese. *Appl.*
569 *Envir. Microbiol.* 54, 1472–1480.

570 Lovley, D.R., Phillips, E.J.P., 1986. Availability of Ferric Iron for Microbial Reduction in
571 Bottom Sediments of the Freshwater Tidal Potomac River. *Appl. Envir. Microbiol.* 52,
572 751–757.

573 Magnetite - www.mindat.org [WWW Document], 2001. URL <http://www.mindat.org/min-2538.html>

575 Moon, J.-W., Rawn, C.J., Rondinone, A.J., Wang, W., Vali, H., Yeary, L.W., Love, L.J.,
576 Kirkham, M.J., Gu, B., Phelps, T.J., 2010. Crystallite Sizes and Lattice Parameters of
577 Nano-Biomagnetite Particles. *J. Nanosci. Nanotechnol.* 10, 8298–8306.

578 Morris, R. V., Klingelh fer, G., Schr er, C., Fleischer, I., Ming, D.W., Yen, A.S., Gellert,
579 R., Arvidson, R.E., Rodionov, D.S., Crumpler, L.S., Clark, B.C., Cohen, B.A.,
580 McCoy, T.J., Mittlefehldt, D.W., Schmidt, M.E., De Souza, J.A., Squyres, S.W., 2008.

581 Iron mineralogy and aqueous alteration from Husband Hill through Home Plate at

582 Gusev Crater, Mars: Results from the Mössbauer instrument on the Spirit Mars
583 Exploration Rover. *J. Geophys. Res. E Planets* 113.

584 Morris, R. V, Klingelhöfer, G., Bernhardt, B., Schröder, C., Rodionov, D.S., de Souza,
585 P.A., Yen, A., Gellert, R., Evlanov, E.N., Foh, J., Kankeleit, E., Gütlich, P., Ming,
586 D.W., Renz, F., Wdowiak, T., Squyres, S.W., Arvidson, R.E., 2004. Mineralogy at
587 Gusev Crater from the Mössbauer Spectrometer on the Spirit Rover. *Science* (80-.).
588 305, 833 LP-836.

589 Morris, R. V, Klingelhöfer, G., Schröder, C., Rodionov, D.S., Yen, A., Ming, D.W., de
590 Souza, P.A., Fleischer, I., Wdowiak, T., Gellert, R., Bernhardt, B., Evlanov, E.N.,
591 Zubkov, B., Foh, J., Bonnes, U., Kankeleit, E., Gütlich, P., Renz, F., Squyres, S.W.,
592 Arvidson, R.E., 2006. Mössbauer mineralogy of rock, soil, and dust at Gusev crater,
593 Mars: Spirit's journey through weakly altered olivine basalt on the plains and
594 pervasively altered basalt in the Columbia Hills. *J. Geophys. Res. Planets* 111, n/a--
595 n/a. doi:10.1029/2005JE002584

596 Morris, R. V, Ruff, S.W., Gellert, R., Ming, D.W., Arvidson, R.E., Clark, B.C., Golden,
597 D.C., Siebach, K., Klingelhöfer, G., Schröder, C., Fleischer, I., Yen, A.S., Squyres,
598 S.W., 2010. Identification of Carbonate-Rich Outcrops on Mars by the Spirit Rover.
599 *Sci.* 329, 421–424. doi:10.1126/science.1189667

600 Nixon, S.L., Cockell, C.S., Tranter, M., 2012. Limitations to a microbial iron cycle on
601 Mars. *Planet. Space Sci.* 72, 116–128. doi:10.1016/j.pss.2012.04.003

602 O'Loughlin, E.J., Gorski, C.A., Scherer, M.M., Boyanov, M.I., Kemner, K.M., 2010.
603 Effects of Oxyanions, Natural Organic Matter, and Bacterial Cell Numbers on the

604 Bioreduction of Lepidocrocite (γ -FeOOH) and the Formation of Secondary
605 Mineralization Products. *Environ. Sci. Technol.* 44, 4570–4576.
606 doi:10.1021/es100294w

607 Parenteau, M.N., Jahnke, L.L., Farmer, J.D., Cady, S.L., 2014. Production and Early
608 Preservation of Lipid Biomarkers in Iron Hot Springs. *Astrobiology* 14, 502–521.
609 doi:10.1089/ast.2013.1122

610 Pereira, B.G., Vianna-Soares, C.D., Righi, A., Pinheiro, M.V.B., Flores, M.Z.S., Bezerra,
611 E.M., Freire, V.N., Lemos, V., Caetano, E.W.S., Cavada, B.S., 2007. Identification of
612 lamivudine conformers by Raman scattering measurements and quantum chemical
613 calculations. *J. Pharm. Biomed. Anal.* 43, 1885–1889.

614 Perez-Gonzalez, T., Jimenez-Lopez, C., Neal, A.L., Rull-Perez, F., Rodriguez-Navarro, A.,
615 Fernandez-Vivas, A., Iañez-Pareja, E., 2010. Magnetite biomineralization induced by
616 *Shewanella oneidensis*. *Geochim. Cosmochim. Acta* 74, 967–979.
617 doi:10.1016/j.gca.2009.10.035

618 Piepenbrock, A., Dippon, U., Porsch, K., Appel, E., Kappler, A., 2011. Dependence of
619 microbial magnetite formation on humic substance and ferrihydrite concentrations.
620 *Geochim. Cosmochim. Acta* 75, 6844–6858. doi:10.1016/j.gca.2011.09.007

621 Rietveld, H.M., 1969. A profile refinement method for nuclear and magnetic structures. *J.*
622 *Appl. Crystallogr.* 2, 65–71. doi:10.1107/S0021889869006558

623 Rodríguez-Carvajal, J., 1993. Recent advances in magnetic structure determination by
624 neutron powder diffraction. *Phys. B Condens. Matter* 192, 55–69.
625 doi:http://dx.doi.org/10.1016/0921-4526(93)90108-I

626 Rothschild, L.J., Mancinelli, R.L., 2001. Life in extreme environments. *Nature* 409, 1092–
627 1101.

628 Ruecker, A., Schröder, C., Byrne, J., Weigold, P., Behrens, S., Kappler, A., 2016.
629 Geochemistry and Mineralogy of Western Australian Salt Lake Sediments:
630 Implications for Meridiani Planum on Mars. *Astrobiology* 16, 525–538.
631 doi:10.1089/ast.2015.1429

632 Rull, F., Martinez-Frias, J., Rodríguez-Losada, J.A., 2007. Micro-Raman spectroscopic
633 study of El Gasco pumice, western Spain. *J. Raman Spectrosc.* 38, 239–244.
634 doi:10.1002/jrs.1628

635 Rull, F., Martinez-Frias, J., Sansano, A., Medina, J., Edwards, H.G.M., 2004. Comparative
636 micro-Raman study of the Nakhla and Vaca Muerta meteorites. *J. Raman Spectrosc.*
637 35, 497–503. doi:10.1002/jrs.1177

638 Sansano-Caramazana, A., 2015. Síntesis y caracterización espectroscópica de sulfatos de
639 hierro: implicaciones en astrobiología y la exploración de Marte. University of
640 Valladolid.

641 Sansano, A., Navarro, R.J., Manrique, J.A., Medina, J., Rull, F., 2015. Multispectral
642 Analysis of Mars Analog Altered Volcanic Materials from Faroe Islands. Implications
643 for Missions as ExoMars and Mars 2020. *Lunar Planet. Sci. Conf.*

644 Scherrer, P., 1918. Bestimmung der Grösse und der inneren Struktur von Kolloidteilchen
645 mittels Röntgenstrahlen. *Nachrichten von der Gesellschaft der Wissenschaften zu*
646 *Göttingen, Math. Klasse* 1918, 98–100. doi:10.1007/978-3-662-33915-2

647 Schröder, C., 2003. ATHENA Reference Samples. Mainz.

648 Shebanova, O.N., Lazor, P., 2003. Raman spectroscopic study of magnetite (FeFe₂O₄): a
649 new assignment for the vibrational spectrum. *J. Solid State Chem.* 174, 424–430.
650 doi:10.1016/S0022-4596(03)00294-9

651 Stookey, L.L., 1970. Ferrozine---a new spectrophotometric reagent for iron. *Anal. Chem.*
652 42, 779–781.

653 Vandenberghe, R.E., Barrero, C.A., da Costa, G.M., Van San, E., De Grave, E., 2000.
654 Mössbauer characterization of iron oxides and (oxy)hydroxides: the present state of
655 the art. *Hyperfine Interact.* 126, 247–259. doi:10.1023/A:1012603603203

656 Veeramani, H., Alessi, D.S., Suvorova, E.I., Lezama-Pacheco, J.S., Stubbs, J.E., Sharp,
657 J.O., Dippon, U., Kappler, A., Bargar, J.R., Bernier-Latmani, R., 2011. Products of
658 abiotic U(VI) reduction by biogenic magnetite and vivianite. *Geochim. Cosmochim.*
659 *Acta* 75, 2512–2528. doi:10.1016/j.gca.2011.02.024

660 Wang, A., Korotev, R.L., Jolliff, B.L., Ling, Z., 2015. Raman imaging of extraterrestrial
661 materials. *Planet. Space Sci.* 112, 23–34. doi:10.1016/j.pss.2014.10.005

662 Wohlfarth, E.P., Arrott, A.S., 1982. *Ferromagnetic Materials: A Handbook on the*
663 *Properties of Magnetically Ordered Substances*, Vols. 1 and 2, Physics Today.
664 doi:10.1063/1.2914974

665 Zegeye, A., Abdelmoula, M., Usman, M., Hanna, K., Ruby, C., 2011. In situ monitoring of
666 lepidocrocite bioreduction and magnetite formation by reflection Mössbauer
667 spectroscopy. *Am. Mineral.* 96, 1410–1413. doi:10.2138/am.2011.3794

668 Zegeye, a, Mustin, C., Jorand, F., 2010. Bacterial and iron oxide aggregates mediate
669 secondary iron mineral formation: green rust versus magnetite. *Geobiology* 8, 209–22.

670 doi:10.1111/j.1472-4669.2010.00238.x

671

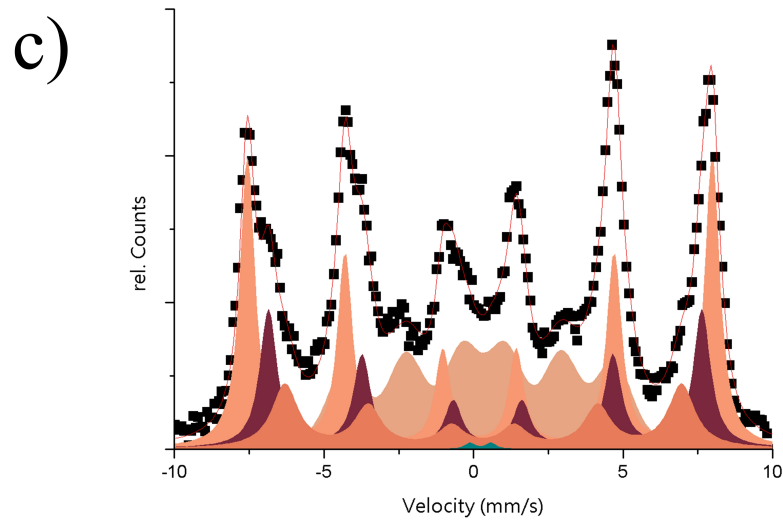
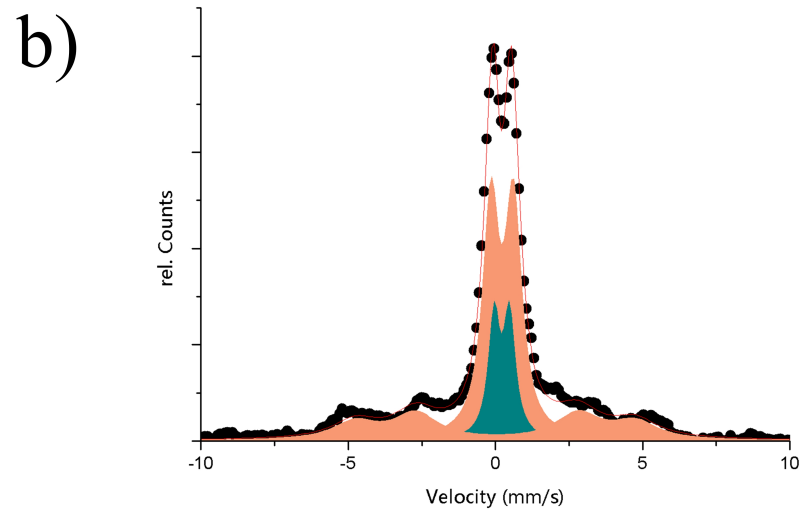
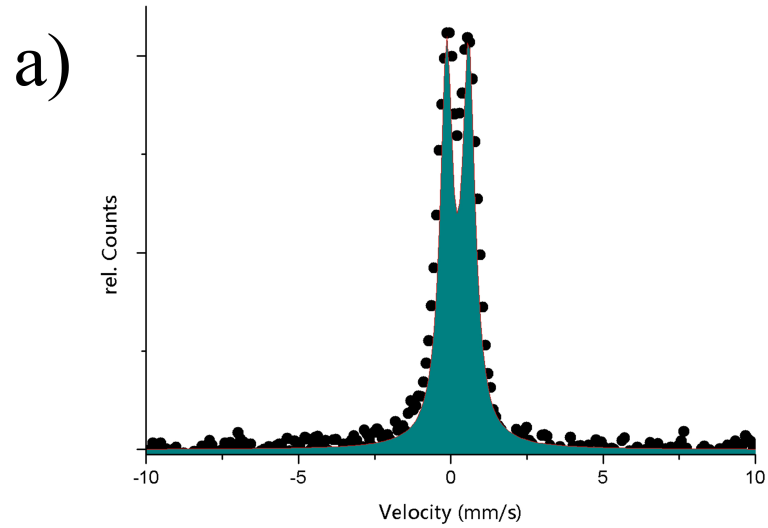
List of Figure

Figure 1 - MIMOS II analysis from the 2014 experiments (a) in situ measurement 6 hours after start FH-AQDS on the MIMOS II, (b) in situ measurement 19 days after start FH-AQDS on the MIMOS II, (c) filtered sample room temperature FH-AQDS.

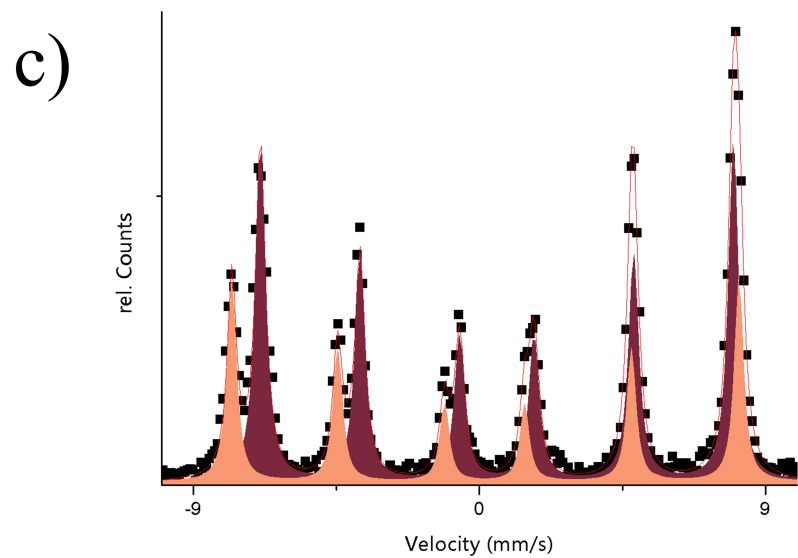
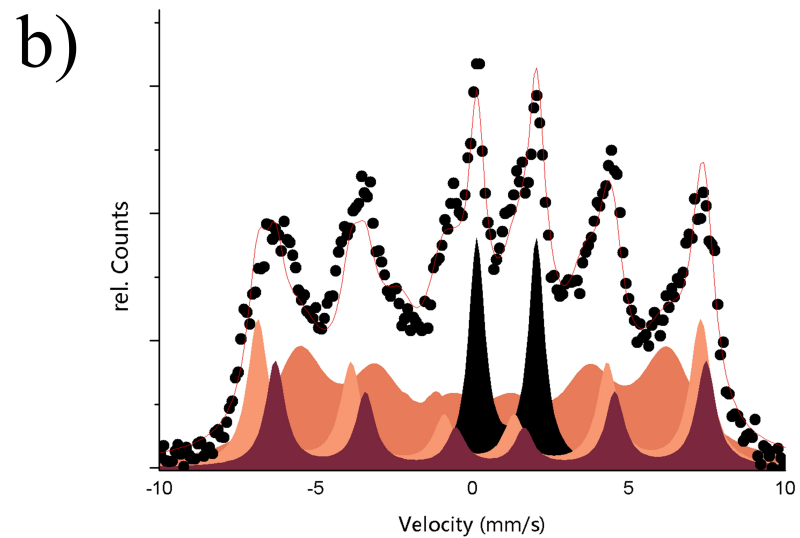
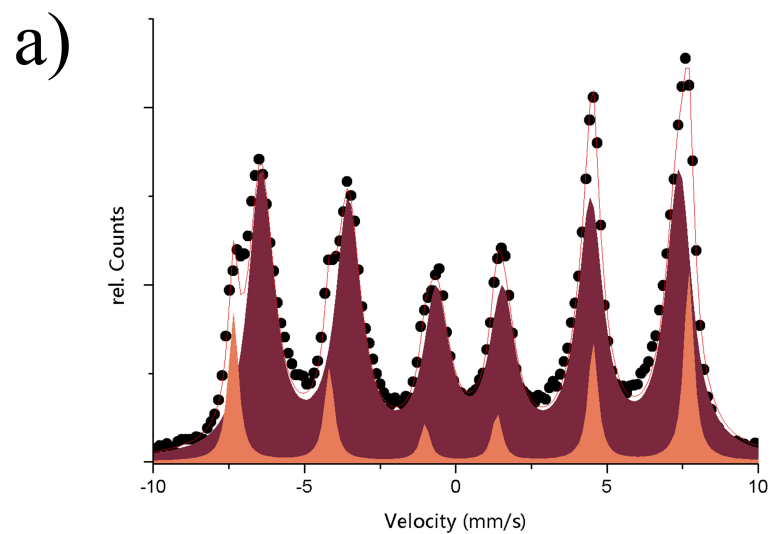
Figure 2 - MIMOS II analysis from the 2013 experiments (a) FH-AQDS measured at room temperature; (b) FH+AQDS measured at room temperature; (c) Magnetite (Athena Reference Sample 043).

Figure 3 - XRD pattern for FH-AQDS and FH+AQDS. Samples show a broad reflection between 5° and 15° 2θ due to the Kapton film (Kp) in which they were sealed.

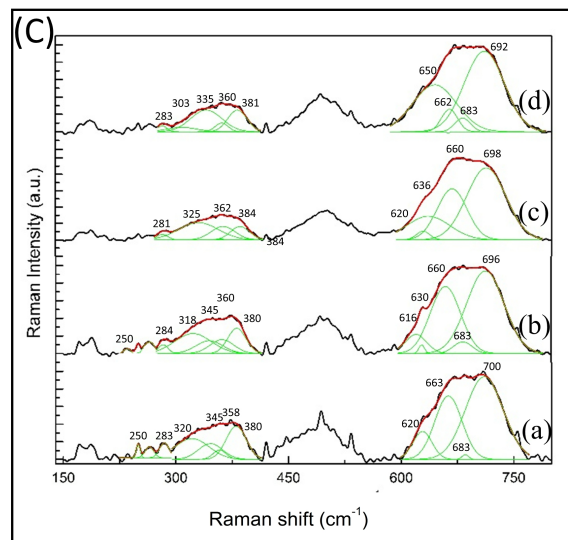
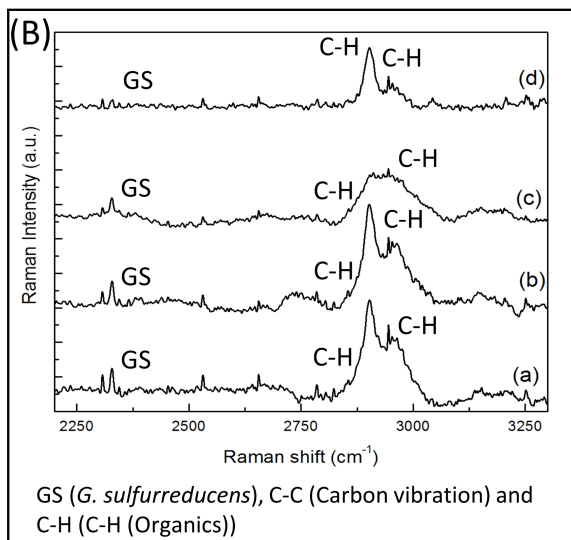
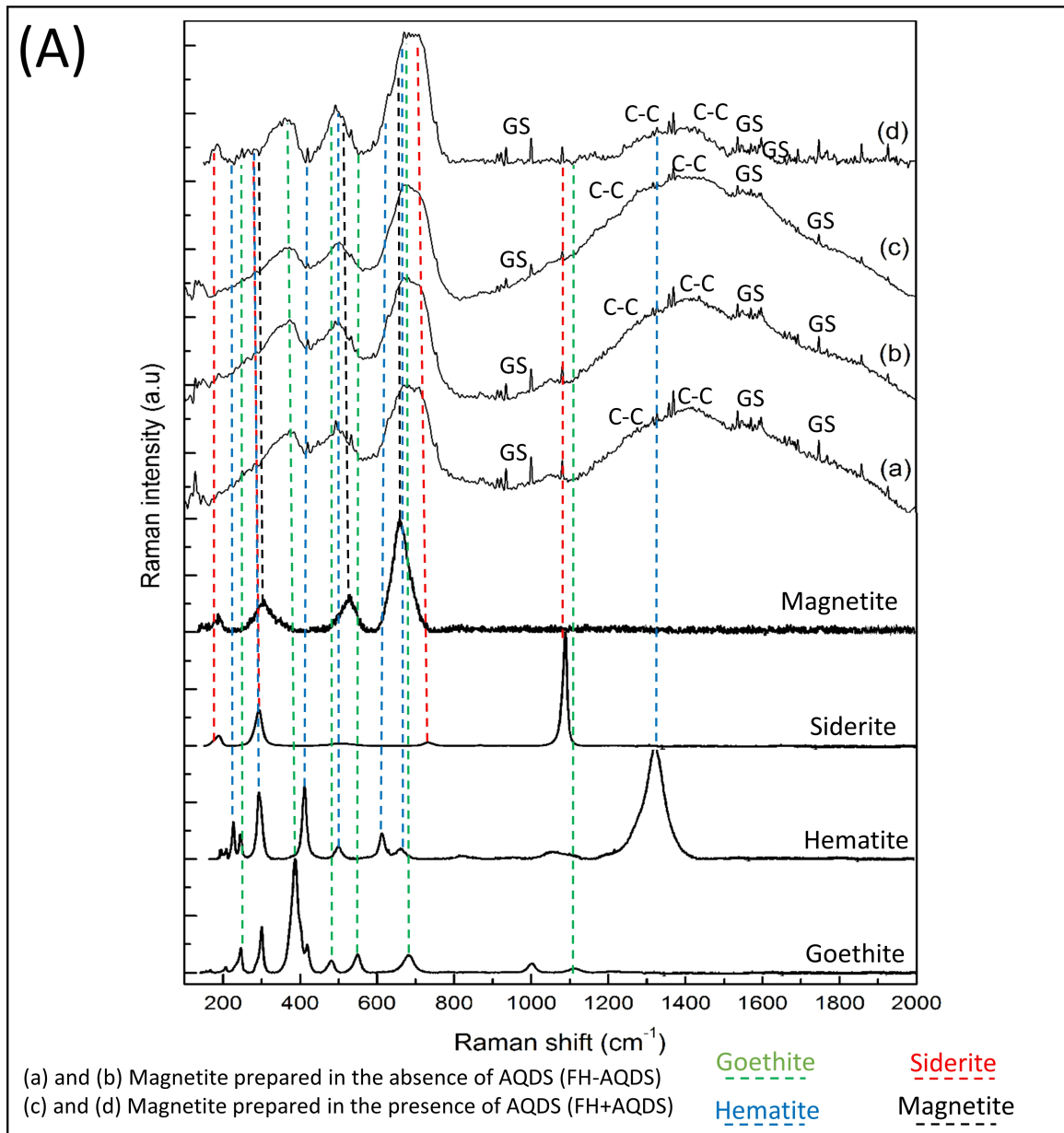
Figure 4. (A) Raman Spectra from 100 to 2000 cm^{-1} of (a) and (b) Magnetite prepared in the absence of AQDS (FH-AQDS); (c) and (d) Magnetite prepared in the presence of AQDS (FH+AQDS). Assignment of the most intense Raman vibration: Hematite, Magnetite, Goethite, Siderite, GS (G. sulfurreducens) and C-C (Carbon vibration). (B) Raman spectra from 2000 to 3000 cm^{-1} of (a) and (b) Magnetite prepared in the absence of AQDS (FH-AQDS); (c) and (d) Magnetite prepared in the presence of AQDS (FH+AQDS). Assignment of the most intense Raman vibration: C-H (C-H (Organics) and GS (G. sulfurreducens). (C) Gaussian band fitting of the regions: 200-420 cm^{-1} and 600 to 800 cm^{-1} .



- Data
- Magnetite (tet^{3+})
- Magnetite ($\text{oct}^{2.5+}$)
- Goethite nanophase
- Magnetite nanophase
- Ferrihydrite
- Siderite
- Fit



- Data
- Magnetite (tet^{3+})
- Magnetite ($\text{oct}^{2.5+}$)
- Magnetite nanophase
- Siderite
- Fit



List of Tables:

Table 1. Mössbauer parameters of experimental and Martian samples.

Table 2. Bands used as diagnostic for the curve fitting identification of principal iron oxide phases.

Table 3. (a) Raman general position in curve fitting of the Raman spectra from FH+AQDS-13 and FH-AQDS-13 samples. (b) Raman Curve analysis per spectra corresponding to Figure 3 and its possible mineral assignments compared to standards.

Table 4. Comparison of the main features of Mössbauer, XRD, and Raman that can be used for potential bio-mineral detection.

Table 1

Sample	Mineral Phase	CS (δ) mm s ⁻¹	Linewidth (S) mm s ⁻¹	ΔE_Q mm s ⁻¹	B_{hf} T	Relative area %	Fe(II)/Fe(III) in Fe ₃ O ₄	
FH-AQDS-14 (<i>in situ</i> , 6 h)	Ferrihydrite	0.34	0.25	0.74		100		
FH-AQDS-14 (<i>in situ</i> , 19 days)	Ferrihydrite	0.34	0.34	0.77		11.4		
	Magnetite nanophase ^a	0.33	0.24	0.53		21.7		
	Magnetite nanophase ^b	0.13	0.92	-0.03	29.5	66.9		
FH-AQDS-14 (filtered)	Ferrihydrite	0.34	0.20	0.74		0.5		
	Magnetite (tet- Fe ³⁺)	0.30	0.30	0.00	48.1	40.1		
	Magnetite (oct- Fe ^{2,5+})	0.54	0.34	- 0.04	44.9	21.7		
	Magnetite nanophase ^b	0.43	0.54	0.00	41.2	15.8		
	Goethite nanophase	0.39	0.35	-0.06	27.6	21.9		
FH-AQDS-13 (filtered)	Magnetite (tet-Fe ³⁺)		0.30	0.19	0.00	46.6	20.8	
	Magnetite (oct- Fe ^{2,5+})		0.56	0.52	-0.00	42.8	79.2	0.65
FH+AQDS-13	Magnetite (tet-Fe ³⁺)		0.33	0.40	0.00	44.0	18.6	
	Magnetite (oct- Fe ^{2,5+})		0.69	0.36	0.01	42.8	12.1	0.25
	Magnetite nanophase ^b		0.45	1.07	0.01	36.6	35.7	
	Magnetite nanophase ^b		0.71	0.59	0.04	18.0	11.4	
	Siderite		1.21	0.31	1.90		22.2	
Athena Reference Sample 043	Magnetite (tet-Fe ³⁺)		0.29	0.2	0.01	49.4	37.1	
	Magnetite (oct- Fe ^{2,5+})		0.66	0.2	0.00	46.1	62.9	0.46
Average Mars magnetite ^c	Magnetite (tet-Fe ³⁺)		0.31±0.03		0.01±0.03	50.0±0.5		
	Magnetite (oct- Fe ^{2,5+})		0.66±0.06		-0.01±0.08	46.7±0.8		
Average Mars goethite ^c	Goethite		0.38±0.02		-0.19±0.10	37.3±2.9		

^aSuperparamagnetic magnetite - magnetic ordering prevented by small particle size.

^bMagnetically ordered magnetite that has not reached full hyperfine splitting because of small particle size and/or impurities

^c**Values from Morris et al. (2008), averaging all magnetite and goethite measurements obtained in Gusev Crater with Mars Exploration Rover Spirit. Uncertainties quoted are standard deviations (2σ).**

Table 2.

Mineral Phase	Principal Raman bands (cm ⁻¹)
Goethite	244, 299, 385 , 480, 681
Hematite	225 , 245, 290-300, 412
Lepidocrocite	250 , 348, 379, 528, 650
Siderite	184, 287, 722, 1082
Ferrihydrite	370, 510, 710
Magnetite	310, 540, 670
Maghemite	350, 512, 665 , 730

Table 3 a.

Raman band position (cm ⁻¹)	Raman assignment
172 (w)	*****
186 (w)	Siderite
283 (m)	Hematite/Goethite/Siderite
340 (m)	Magnetite
378 (m)	Hematite/Goethite
420 (vw)	Goethite
451 (sh)	****
474 (m)	Goethite
495 (s)	Siderite/Magnetite
533 (sh)	Magnetite
650 (sh)	****
667 (vs)	Magnetite
717 (vs)	Siderite
755 (sh)	<i>G. sulfurreducens</i>
1000 (w)	<i>G. sulfurreducens</i>
1082 (w)	Siderite
1314 (m)	Hematite/Goethite
1358 (w)	<i>G. sulfurreducens</i>
1370 (w)	<i>G. sulfurreducens</i>
1422 (m)	Carbon vibration
1565 (m)	Carbon vibration
1598 (w)	<i>G. sulfurreducens</i>
2328 (w)	<i>G. sulfurreducens</i>
2903 (s)	C-H(Organics)
2961 (m)	C-H (Organics)

**** Raman band not assigned

Table 3 b.

Mineral	Principal Raman fitting bands (cm ⁻¹) of the Mineral and organics detected			
Phase	Raman Spectra (a)	Raman spectra (b)	Raman spectra (c)	Raman Spectra (d)
Goethite	283, 376 , 420, 475	284, 373 , 471	285, 383 , 420	283, 385 , 420, 480
Hematite	250 , 283, 493, 609, 1348	250 , 283, 401, 497, 609, 1337	250 , 283, 403, 480, 1358	250 , 283, 491, 609, 1331
Siderite	187 , 505, 711, 1083	188 , 504, 703, 1083	187 , 700, 1083	184 , 712, 1083
Magnetite	308, 533, 653 or 691 (<i>bio-mag</i>)*	315, 534, 652 or 679 (<i>bio-mag</i>)*	308, 534, 642 or 685 (<i>bio-mag</i>)*	315, 533, 652 or 690 (<i>bio-mag</i>)*
Organics	1327, 1370 , 1400, 1537, 1598 , 2328, 2344, 2884, 2902 , 2963	1279, 1386 , 1431, 1549, 1598 , 2307, 2328, 2874, 2902, 2963	1287 , 1427, 1559, 1600 , 2328, 2878, 2905 , 2940, 2974	1270, 1401 , 1438, 1469, 1542, 1597 , 2874, 2903 , 2947, 2969 , 3043

*Refers to the magnetite produced by *G. sulfurreducens*. The curve fitting relative band intensity of I₆₈₅₋₉₀/I₆₅₀ shows for: (a) ~1.50, (b) 1.27, (c) 1.63, (d) 1.2.

Table 4.

Technique	Structure and crystallinity	Particle size	Detection of organics	Oxidation states	Stoichiometry	*Geological context
Raman spectroscopy	Yes	No	Yes	No	Potentially	Yes
XRD	Yes	Yes	No	No	No	Potentially
Mössbauer Spectroscopy ^a	Yes	Yes	No	Fe	Yes	Yes

^aMössbauer spectroscopy is limited to Fe-bearing materials.

*Geological Context: Mineral assemblages and accompanying minerals